Applied Mathematics, Modeling and Computer Simulation
C.-H. Chen et al. (Eds.)

doi:10.3233/ATDE221022

Effect of Transmission Lines Arrangement on Drag and Lift Coefficients: A Numerical Study

Chao ZHOU[a], Hui LIU[a] and Fangqing ZHANG[b,1]

[a]*Electric Power Research Institute of State Grid Shandong Electric Power Company, Jinan 250002, China*
[b]*Wuhan Relabo Technology Company, Wuhan 430000, China*

Abstract. The safety of transmission lines is affected significantly by wind deflection characteristics. In the present study, the effect of transmission lines arrangement on wind deflection characteristics is investigated, where the distance between transmission lines is different. At low Re, the effect of the distance between transmission lines on C_{Drag} and C_{Lift} is significant. C_{Drag} of the left two transmission lines are the same, which are larger, while C_{Drag} of the right two transmission lines are smaller. C_{Lift} of the top two transmission lines are larger, while C_{Lift} of the bottom two transmission lines are smaller. With the distance between the transmission lines increasing, the interaction between the transmission lines becomes weak, both C_{Drag} and C_{Lift} of the four transmission lines approach to those of the single transmission line.

Keywords. Transmission lines arrangement, wind deflection characteristics, drag and lift coefficients, lattice Boltzmann method

1. Introduction

The stable supply of the electric power is very important. However, the safety of transmission lines is affected significantly by the wind deflection characteristics. Therefore, the effect of the wind deflection characteristics on transmission lines is studied widely [1-12]. Tokoro investigated the basic aerodynamic characteristics of twin cable through a series of wind tunnel tests employing full aero elastic twin cable model [2]. Matsumoto described the mechanism of dry galloping of inclined cable of cable-stayed bridges in relation to Karman vortex mitigation [4]. Asgarian evaluated the progressive collapse vulnerability of a lattice tower in a 400 kV power transmission line [6]. Damatty conducted an extensive parametric study on a number of transmission line systems to evaluate their critical response to downburst loads [8]. Jafari incorporated an extensive review based on the existing papers about different sources of wind-induced cable vibration consisting of vortex-induced vibration, rain-wind-induced vibration, dry galloping, ice galloping, and wake galloping [10].

---

1 Corresponding Author, Fangqing ZHANG, Wuhan Relabo Technology Company, Wuhan 430000, China; E-mail: zhangfangqing@relabo.cn

Though the wind deflection characteristics are studied widely, the effect of transmission lines arrangement on the wind deflection characteristics is rare. Under various transmission lines arrangements, C_{Drag} and C_{Lift} on transmission lines are quite different, which affect the wind deflection characteristics directly. Therefore, to deepen the understanding of the wind deflection characteristics, studying the effect of transmission lines arrangement on the wind deflection characteristics is necessary.

The present paper includes the following parts. The first part is the problem description, and the second part is the numerical method introduction. Next, to simulate the problem accurately, the grid convergence test is conducted, where four groups of grids are compared. Then, C_{Drag} and C_{Lift} under various transmission lines arrangements are discussed, where the distance between transmission lines are different. Lastly, the present paper is concluded.

2. Problem Description

To study the effect of transmission lines arrangement on the wind deflection characteristics, a typical transmission lines type is adopted, namely, quad split transmission lines. To simplify the problem, four transmission lines are described by four cylinders, as shown in figure 1. The diameter of the cylinders is D, and the size of the computational domain is $\mathrm{W} \times \mathrm{H} = 60\mathrm{D} \times 28\mathrm{D}$.To represent various transmission lines arrangements, the distance between transmission lines are different, namely, the distance between the transmission lines is different, which is denoted by Δ. The Reynolds number is a key dimensionless number, which is defined by Re=DU/ν, where U is the inlet velocity, ν is the kinematic viscosity of the fluid. In the present study, Re is kept at 40, where the fluid flow is steady.

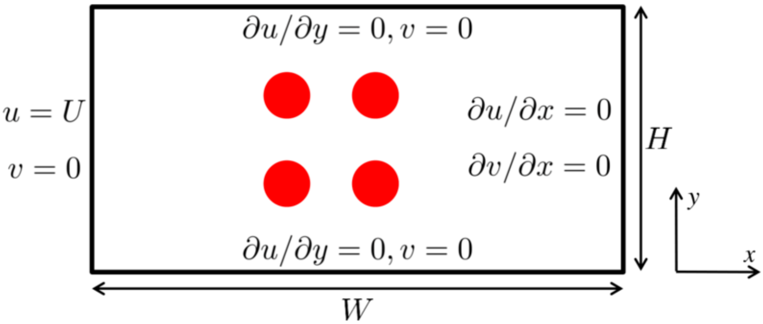

Figure 1. Quad split transmission lines.

3. Numerical Method

To calculate the flow, the Navier-Stokes equations are adopted, namely,

$$\frac{\partial \rho}{\partial t} + \nabla \cdot (\rho \mathrm{u}) = 0$$

$$\frac{\partial \mathrm{u}}{\partial t} + (\mathrm{u} \cdot \nabla \mathrm{u}) = -\frac{1}{\rho} \nabla p + \nu \nabla^2 \mathrm{u}$$

where ρ is the fluid density, u is the fluid velocity, and p is the fluid pressure. To calculate the flow, the lattice Boltzmann method is adopted [13-24], whose evolution equation is

$$f_i(\mathrm{x}+\mathrm{c}_i\Delta t, t+\Delta t) - f_i(\mathrm{x}, t) = -\frac{1}{\tau}\left(f_i - f_i^{eq}\right)$$

where $f_i(x,t)$ is the distribution function, f_i^{eq} is the equilibrium distribution function, τ is the dimensionless relaxation time. The D2Q9 model [25-28] is adopted, whose equilibrium distribution function is

$$f_i^{eq}(\rho,\mathrm{u}) = w_i\rho\left[1 + \frac{\mathrm{c}_i\cdot\mathrm{u}}{c_s^2} + \frac{(\mathrm{c}_i\cdot\mathrm{u})^2}{2c_s^4} - \frac{\mathrm{u}\cdot\mathrm{u}}{2c_s^2}\right]$$

where w_i is the weight coefficient of the distribution function, and c_i is the discrete velocity vector of the distribution function. Lastly, the fluid density and velocity are calculated by

$$\rho = \sum_i f_i$$

$$\mathrm{u} = \frac{1}{\rho}\sum_i \mathrm{c}_i f_i$$

4. Grid Independence Test

To simulate the problem accurately, the grid independence test is important, and we adopt four grid resolutions, namely, $\mathbf{D/\Delta x}$=12, 24, 36, 48. To simplify the grid independence test, a single cylinder is placed in the computational domain. Figure 2 shows $\boldsymbol{C_{Drag}}$ and $\boldsymbol{C_{Lift}}$ at different grid resolutions, where $\boldsymbol{C_{Drag}}$ and $\boldsymbol{C_{Lift}}$ are calculated by

$$\boldsymbol{C}_{\mathrm{Drag}} = \frac{\mathbf{2}\boldsymbol{F}_{\mathrm{Drag}}}{\boldsymbol{\rho D^2 U^2}}$$

$$\boldsymbol{C}_{\mathrm{Lift}} = \frac{\mathbf{2}\boldsymbol{F}_{\mathrm{Lift}}}{\boldsymbol{\rho D^2 U^2}}$$

where $\boldsymbol{F}_{\mathrm{Drag}}$ and $\boldsymbol{F}_{\mathrm{Lift}}$ are the drag and lift forces. Since Re is low, the fluid flow is steady, and $\boldsymbol{C_{Drag}}$ and $\boldsymbol{C_{Lift}}$ keep constant. At different grid resolutions, $\boldsymbol{C}_{\mathrm{Drag}}$ varies significantly. With the grid resolution increasing, $\boldsymbol{C}_{\mathrm{Drag}}$ decreases until it varies negligibly. The difference between $\boldsymbol{D/\Delta x} = \mathbf{36}$ and 48 is negligible, which represents that the grid independence is achieved. $\boldsymbol{C_{Lift}}$ is not sensitive to the grid resolution, namely, $\boldsymbol{C}_{\mathrm{Lift}}$ is always zero at different grid resolutions. Therefore, we adopt the grid resolution $\boldsymbol{D/\Delta x} = \mathbf{36}$ in the following simulations. Figure 3 shows the distribution of the vortex magnitude around the transmission line. The fluid flow is steady, the vortex is attached to the rear, and no vortex shedding occurs.

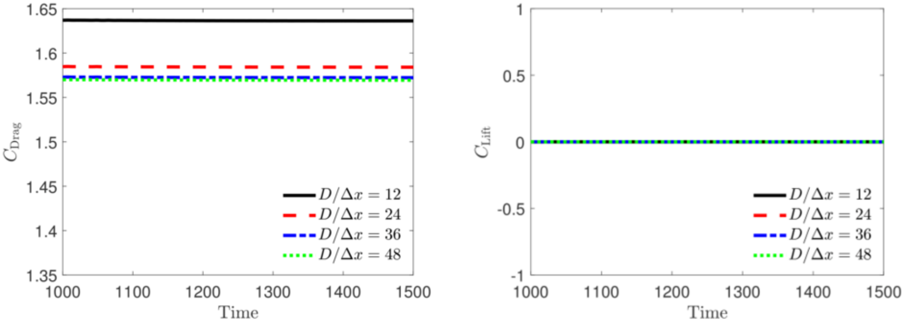

(a)Drag Coefficient (b)Lift Coefficient

Figure 2. $\boldsymbol{C_{Drag}}$ and $\boldsymbol{C_{Lift}}$ at different grid resolutions.

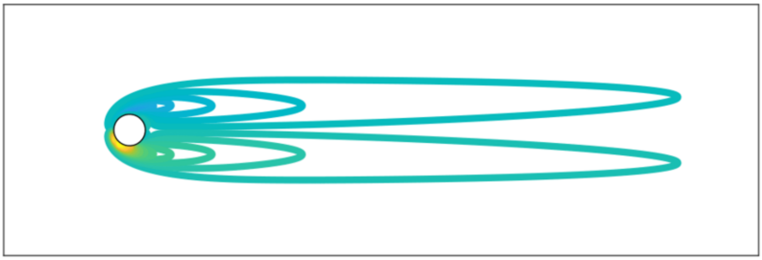

Figure 3. Distribution of the vortex magnitude.

5. Results and Discussions

Then, the effect of transmission lines arrangement on the wind deflection characteristics is studied. Four transmission lines arrangements are adopted, where the distance between transmission lines is different, namely, $\Delta = 2D$, $4D$, $8D$, $16D$. Figure 4 shows the distribution of the vortex magnitude, where the distance is different. The effect of the distance between the transmission lines on the fluid flow is significant, which affects C_{Drag} and C_{Lift}. At small Δ, namely, $\Delta = 2D$, the distribution of the vortex magnitude around the four cylinders is like that around the single cylinder. With Δ increasing, the interaction between the lines varies. At large Δ, namely, $\Delta = 16D$, the interaction between the lines becomes very weak, and the distribution of the vortex magnitude around the four lines is almost the same to that around the single line.

Figure 5 shows C_{Drag}, where the distance between the lines is different, together with C_{Drag} of the single line. Though Δ is different, the four lines are divided into two groups, namely, the left two lines and the right two lines. C_{Drag} of the left two lines are the same, which are larger than that of the single line, while C_{Drag} of the right two lines are smaller. With Δ increasing, C_{Drag} of the left two lines decreases, while C_{Drag} of the right two lines increases.

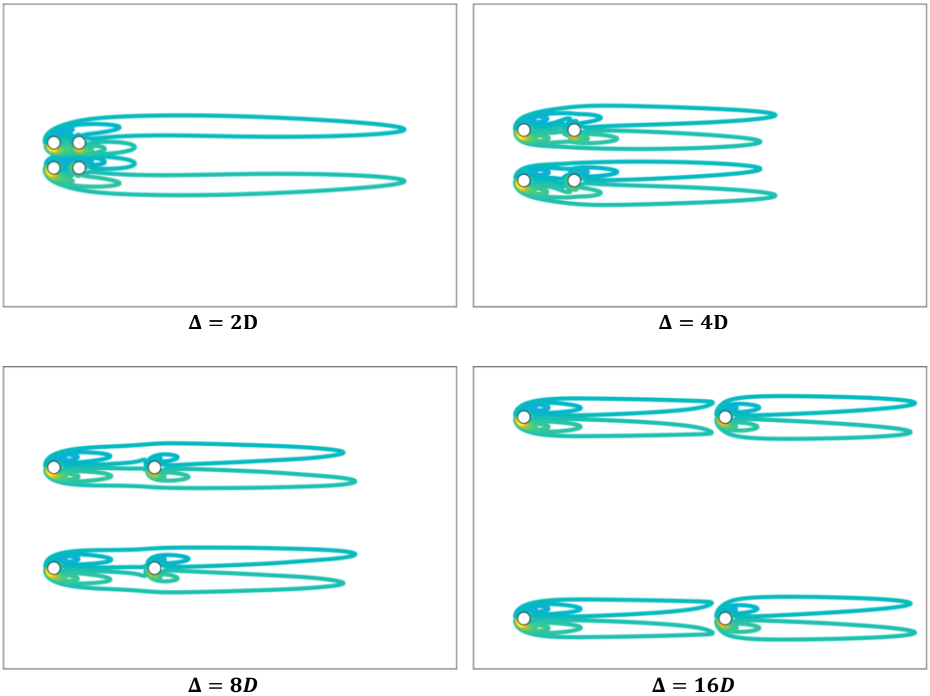

Figure 4. Distribution of the vortex magnitude, where the distance is different.

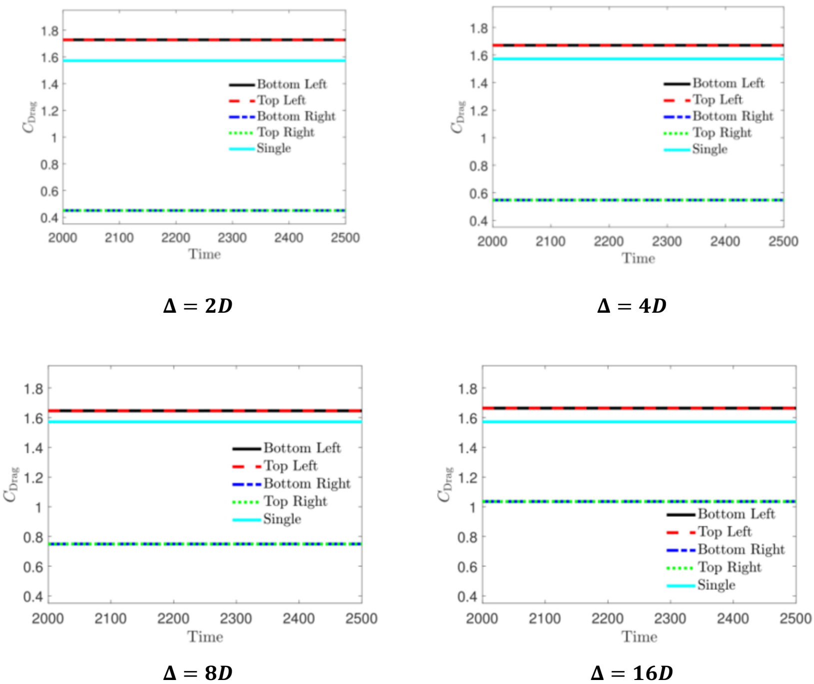

Figure 5. C_{Drag}, where the distance between the lines is different, together with C_{Drag} of the single line.

Figure 6 shows C_{Lift}, where the distance between the lines is different, together with C_{Lift} of the single line. Quite different from C_{Drag}, C_{Lift} of the four lines are divided into another two groups, namely, the top two lines and the bottom two lines. C_{Lift} of the top two lines are larger than that of the single line, while C_{Lift} of the bottom two lines are smaller.

Among the four lines, C_{Lift} of the top left line is the largest, while C_{Lift} of the bottom left line is the smallest. Similar to C_{Drag}, with the increase of Δ, C_{Lift} of the four lines approach to that of the single line. At $\Delta = 16D$, C_{Lift} of the four lines is almost the same to that of the single line, which represents that the interaction between the lines is weak.

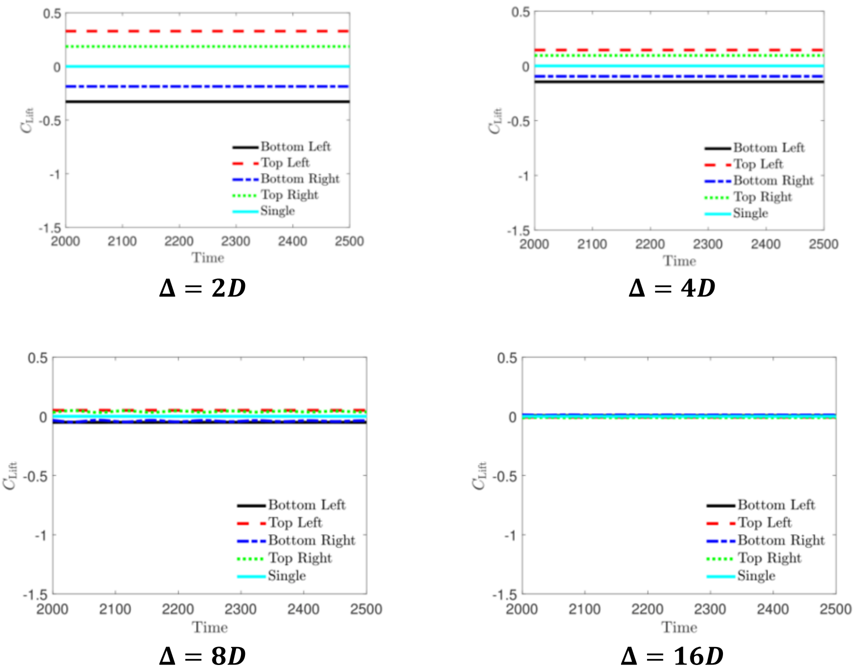

Figure 6. C_{Lift}, where the distance between the lines is different, together with C_{Lift} of the single line.

Furthermore, C_{Drag} and $C_{Lift}$of the four lines at different positions are discussed. Figure 7 shows C_{Drag} of the four lines, where the position of the lines is different, together with C_{Drag} of the single line. Clearly, C_{Drag} of the left two lines are larger than that of the single line, with the increase of Δ, C_{Drag} decreases. However, from $\Delta = 8D$ to $\Delta = 16D$, C_{Drag} appears to increase, which is very surprising. With the increase of Δ, the trend of C_{Drag} of the right two lines is monotonic, namely, C_{Drag} increases gradually.

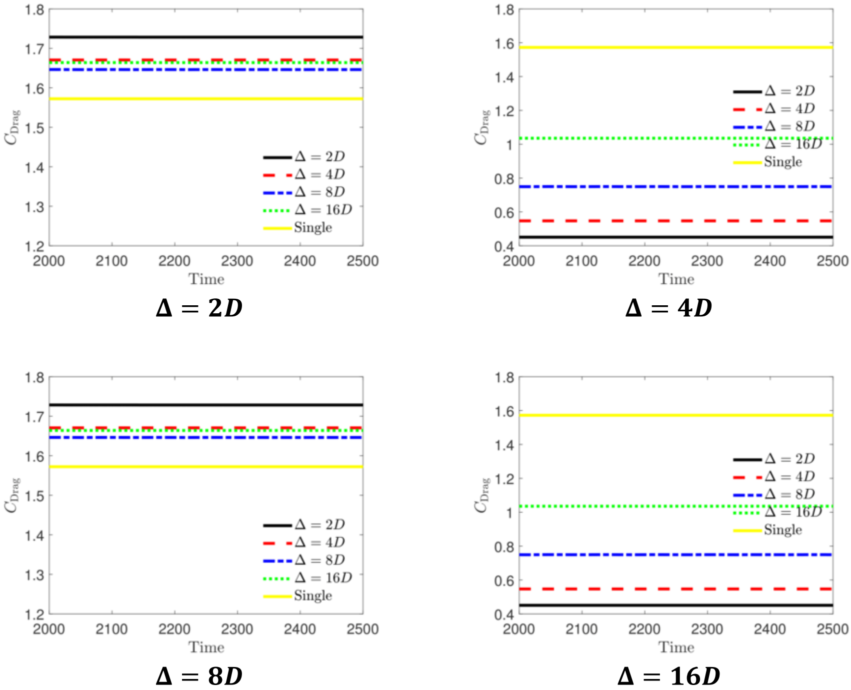

Figure 7. $\boldsymbol{C_{Drag}}$ of the four lines, where the position of the lines is different, together with the drag coefficient of the single line.

Figure 8 shows the time history of C_{Lift} of the four lines, where the position of the lines is different, together with the lift coefficient of the single line. The lift coefficients of the bottom two lines are smaller than that of the single line, and they increase gradually with the increase of Δ. The lift coefficients of the top two lines are larger, and they decrease with the increase of Δ. With the increase of Δ, the lift coefficients of the four lines are monotonic, at Δ=16D, they approach to that of the single line.

6. Conclusions

The effect of transmission lines arrangement on the wind deflection characteristics is investigated with the lattice Boltzmann method. Four transmission lines arrangements are discussed, where the distance between transmission lines is different. With the increase of the distance between the lines, the interaction between the lines becomes weak, the fluid flow around the four lines is closer. C_{Lift} of the left two lines are the same, which are larger, while C_{Drag} of the right two lines are smaller.

C_{Drag} of the top two lines are larger, while C_{Lift} of the bottom two lines are smaller. Both C_{Drag} and C_{Lift} of the four lines approach to the single line with the increase of the distance between the lines.

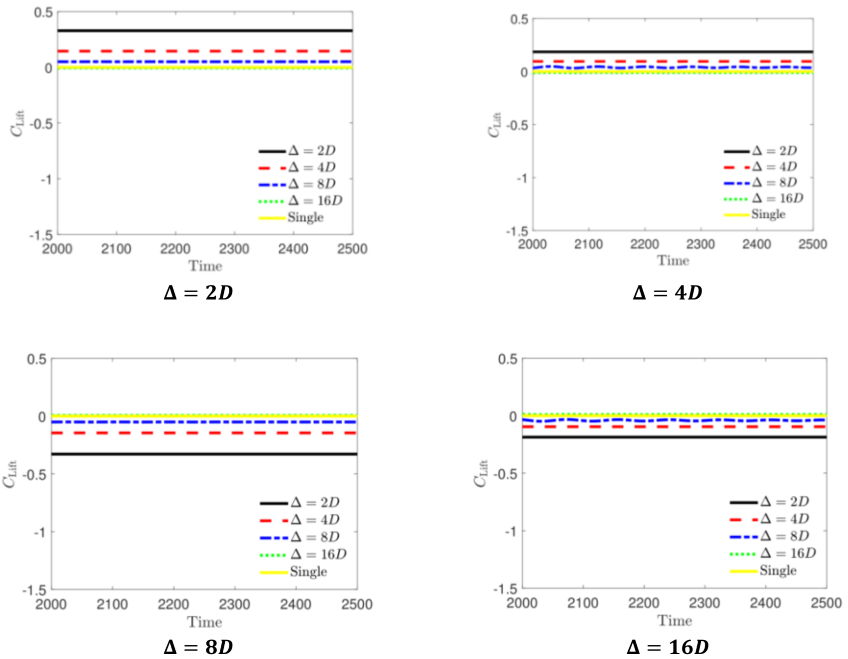

Figure 8. Time history of $\boldsymbol{C_{Lift}}$ of the four lines, where the position of the lines is different, together with $\boldsymbol{C_{Lift}}$ of the single line.

Acknowledgments

The work is supported by 2021A-075 State Grid Shandong Electric Power Company Science and Technology Project Transmission Line Wind Deviation Evaluation and Treatment Method Research.

References

[1] Matsumoto M, Shiraishi N, Kitazawa M, Knisely C, Shirato H, Kim Y, Tsujii M. Aerodynamic behavior of inclined circular cylinders-cable aerodynamics. Journal of Wind Engineering and Industrial Aerodynamics, 1990, 33: 63-72.

[2] Tokoro S, Komatsu H, Nakasu M. A study on wake-galloping employing full aeroelastic twin cable model. Journal of Wind Engineering and Industrial Aerodynamics, 2000, 88: 247-261.

[3] Paluch M, Cappellari T, Riera J. Experimental and numerical assessment of EPS wind action on long span transmission line conductors. Journal of Wind Engineering and Industrial Aerodynamics, 2007, 95: 473-492.

[4] Matsumoto M, Yagi T, Hatsuda H. Dry galloping characteristics and its mechanism of inclined/yawed cables. Journal of Wind Engineering and Industrial Aerodynamics, 2010, 98: 317-327.

[5] Liang S, Zou L, Wang D. Investigation on wind tunnel tests of a full aeroelastic model of electrical transmission tower-line system. Engineering Structures, 2015, 85: 63-72.

[6] Asgarian B, Eslamlou S, Zaghi A. Progressive collapse analysis of power transmission towers. Journal of Constructional Steel Research, 2016, 123: 31-40.

[7] Xie Q, Cai Y, Xue S. Wind-induced vibration of UHV transmission tower line system: Wind tunnel test on aero-elastic model. Journal of Wind Engineering and Industrial Aerodynamics, 2017, 171: 219-229.

[8] Damatty A, Elawady A. Critical load cases for lattice transmission line structures subjected to downbursts: Economic implications for design of transmission lines. Engineering Structures, 2018, 159: 213-226.

[9] Jafari M, Sarkar P. Parameter identification of wind-induced buffeting loads and onset criteria for dry-cable galloping of yawed/inclined cables. Engineering Structures, 2019, 180: 685-699.
[10] Jafari M, Hou F, Abdelkefi A. Wind-induced vibration of structural cables. Nonlinear Dynamics, 2020, 100: 351–421.
[11] Ma L, Khazaali M, Bocchini P. Component-based fragility analysis of transmission towers subjected to hurricane wind load. Engineering Structures, 2021, 242: 112586.
[12] Zhang W, Xiao Y, Li C. Wind load investigation of self-supported lattice transmission tower based on wind tunnel tests. Engineering Structures, 2022, 252: 113575.
[13] Bouzidi M, Firdaouss M, Lallemand P. Momentum transfer of a Boltzmann-lattice fluid with boundaries. Physics of Fluids, 2001, 13: 3452-3459.
[14] Guo Z, Zheng C, Shi B. An extrapolation method for boundary conditions in lattice Boltzmann method. Physics of Fluids, 2002, 14: 2007-2010.
[15] Yin X, Zhang J. An improved bounce-back scheme for complex boundary conditions in lattice Boltzmann method. Journal of Computational Physics, 2012, 231: 4295-4303.
[16] Tao S, Hu J, Guo Z. An investigation on momentum exchange methods and refilling algorithms for lattice Boltzmann simulation of particulate flows. Computers and Fluids, 2016, 133: 1-14.
[17] Hu J, Guo Z. A numerical study on the migration of a neutrally buoyant particle in a Poiseuille flow with thermal convection. International Journal of Heat and Mass Transfer, 2017, 108: 2158-2168.
[18] Frapolli N, Chikatamarla S, Karlin I. Entropic lattice Boltzmann simulation of thermal convective turbulence. Computers & Fluids, 2018, 175: 2-19.
[19] Hu J, Wang L. Migration of a neutrally buoyant particle in a shear flow with thermal convection: A numerical study. International Journal of Heat and Mass Transfer, 2019, 140: 21-24.
[20] Xu A, Shi L, Xi H. Lattice Boltzmann simulations of three-dimensional thermal convective flows at high Rayleigh number. International Journal of Heat and Mass Transfer, 2019, 140: 359-370.
[21] Tao S, Chen B, Xiao H. Lattice Boltzmann simulation of thermal flows with complex geometry using a single-node curved boundary condition. International Journal of Thermal Sciences, 2019, 146: 106112.
[22] Hu J. Motion of a neutrally buoyant circular particle in a clockwise double-lid-driven square cavity. Physics of Fluids, 2020, 32: 113304.
[23] Honari S, Seyedi E. Particulate Modeling of Sand Production Using Coupled DEM-LBM. Energies, 2021, 14: 906.
[24] Shen Z, Yang Z, Abbas M. An Immersed Boundary–Lattice Boltzmann Approach to Study Deformation and Fluid–Structure Interaction of Hollow Sealing Strip. Energies, 2021, 14: 8110.
[25] Qian Y, Humieres D, Lallemand P. Lattice BGK Models for Navier-Stokes Equation. Europhysics Letters, 1992, 17: 479-484.
[26] Chen S, Doolen G. Lattice Boltzmann method for fluid flows. Annual Review of Fluid Mechanics, 1998, 30: 329-364.
[27] Yue L, Chai Z, Wang L. A lattice Boltzmann model for the conjugate heat transfer. International Journal of Heat and Mass Transfer, 2021, 165: 120682.
[28] Christoph R, Ulrich R. An efficient four-way coupled lattice Boltzmann – discrete element method for fully resolved simulations of particle-laden flows. Journal of Computational Physics, 2022, 453: 110942.